Ptychographic coherent diffractive imaging with orthogonal probe relaxation

M. Odstrcil,[1,2,*] P. Baksh,[1] S. A. Boden,[3] R. Card,[1] J. E. Chad,[1] J. G. Frey,[5] and W. S. Brocklesby[1]

[1]*Optoelectronics Research Centre, University of Southampton, SO17 1BJ, UK*
[2]*RWTH Aachen University, Experimental Physics of EUV, JARA-FIT, Steinbachstrasse 15, 52074 Aachen, Germany*
[3]*Faculty of Physical Sciences and Engineering, University of Southampton, Southampton, SO17 1BJ, UK*
[4]*School of Biological Sciences, Faculty of Natural and Environmental Sciences, University of Southampton, Southampton, SO17 1BJ, UK*
[5]*Chemistry, Faculty of Natural and Environmental Sciences, University of Southampton, Southampton, SO17 1BJ, UK*

mo1e13@soton.ac.uk

Abstract: Ptychography is a scanning coherent diffractive imaging (CDI) technique that relies upon a high level of stability of the illumination during the course of an experiment. This is particularly an issue for coherent short wavelength sources, where the beam intensity is usually tightly focused on the sample in order to maximize the photon flux density on the illuminated region of the sample and thus a small change in the beam position results in a significant change in illumination of the sample. We present an improved ptychographic method that allows for limited stability of the illumination wavefront and thus significantly improve the reconstruction quality without additional prior knowledge. We have tested our reconstruction method in a proof of concept experiment, where the beam instability of a visible light source was emulated using a piezo driven mirror, and also in a short wavelength microscopy CDI setup using a high harmonic generation source in the extreme ultraviolet range. Our work shows a natural extension of the ptychography method that paves the way to use ptychographic imaging with any limited pointing stability coherent source such as free electron or soft X-ray lasers and improve reconstruction quality of long duration synchrotron experiments.

OCIS codes: (110.0110) Imaging systems; (040.7480) X-rays, soft x-rays, extreme ultraviolet (EUV); (110.1650) Coherence imaging; (110.4980) Partial coherence in imaging.

#258186 Received 8 Feb 2016; revised 9 Mar 2016; accepted 10 Mar 2016; published 8 Apr 2016

References and links

1. J. Miao, P. Charalambous, J. Kirz, and D. Sayre, "Extending the methodology of x-ray crystallography to allow imaging of micrometre-sized non-crystalline specimens," Nature **400**, 342–344 (1999).
2. H. M. L. Faulkner and J. M. Rodenburg, "Movable aperture lensless transmission microscopy: a novel phase retrieval algorithm," Phys. Rev. Lett. **93**, 023903 (2004).
3. J. M. Rodenburg and H. M. L. Faulkner, "A phase retrieval algorithm for shifting illumination," Appl. Phys. Lett. **85**, 4795–4797 (2004).
4. J. M. Rodenburg, "Ptychography and related diffractive imaging methods," Adv. Imag. Elect. Phys. **150**, 87–184 (2008).
5. P. Thibault and V. Elser, "X-ray diffraction microscopy," Condens. Matt. Phys. **1**,237–255, (2010).
6. J. N. Clark and A. G. Peele, "Simultaneous sample and spatial coherence characterisation using diffractive imaging," Appl Phys, Lett. **99**, 154103 (2011).
7. G. J. Williams, H. M. Quiney, A. G. Peele, and K. A. Nugent, "Coherent diffractive imaging and partial coherence," Phys. Rev. B **75**, 104102 (2007).
8. B. Abbey, L. W. Whitehead, H. M. Quiney, D. J. Vine, G. A. Cadenazzi, C. A. Henderson, K. A. Nugent, E. Balaur, C. T. Putkunz, A. G. Peele and G. J. Williams, "Lensless imaging using broadband x-ray sources," Nature Photonics **5**, 420–424 (2011).
9. P. Thibault and A. Menzel, "Reconstructing state mixtures from diffraction measurements," Nature **494**, 68–71 (2013).
10. L. W. Whitehead, G. J. Williams, H. M. Quiney, D. J. Vine, R. A. Dilanian, S. Flewett, K. A. Nugent, A. G. Peele, E. Balaur, and I. McNulty, "Diffractive imaging using partially coherent x rays," Phys. Rev. Lett. **103**, 243902 (2009).
11. D. H. Parks, X. Shi, and S. D. Kevan, "Partially coherent x-ray diffractive imaging of complex objects," Phys. Rev. A **89**, 063824 (2014).
12. S. Marchesini, A. Schirotzek, C. Yang, H.-t. Wu, and F. Maia, "Augmented projections for ptychographic imaging," Inverse Problems **29**, 115009 (2013).
13. D. J. Batey, D. Claus, and J. M. Rodenburg, "Information multiplexing in ptychography," Ultramicroscopy **138**, 13–21 (2014).
14. A. M. Maiden and J. M. Rodenburg, "An improved ptychographical phase retrieval algorithm for diffractive imaging," Ultramicroscopy **109**, 1256–1262 (2009).
15. N. Halko, P. G. Martinsson, Y. Shkolnisky, and M. Tygert, "An algorithm for the principal component analysis of large data sets," SIAM J. Sci, Comput. **33**, 2580–2594 (2011).
16. J. N. Clark, C. T. Putkunz, E. K. Curwood, D. J. Vine, R. Scholten, I. McNulty, K. A. Nugent, and A. G. Peele, "Dynamic sample imaging in coherent diffractive imaging," Opt. Lett. **36**, 1954–1956 (2011).
17. P. Baksh, M. Odstrčil, H. Kim, S. Boden, J.G. Frey and W.S. Brocklesby, "Wide-field broadband EUV transmission ptychography using a high harmonic source," Opt. Lett. **41**, (in press 2016).
18. M. van Heel and M. Schatz, "Fourier shell correlation threshold criteria," Journal of structural biology **151**, 250–262 (2005).
19. M. Odstrčil, P. Baksh, H. Kim, S. Boden, W. Brocklesby, and J. Frey, "Ultra-broadband ptychography with self-consistent coherence estimation from a high harmonic source," Proc. SPIE **9589**, pp. 958912–958912 (2015).
20. F. Zhang, I. Peterson, J. Vila-Comamala, A. Diaz, F. Berenguer, R. Bean, B. Chen, A. Menzel, I. K. Robinson, and J. M. Rodenburg, "Translation position determination in ptychographic coherent diffraction imaging," Opt. Express **21**, 13592–13606 (2013).
21. R. A. Dilanian, B. O. Chen, S. Teichmann, L. V. Dao, H. M. Quiney, and K. A. Nugent, "High-harmonic-generation spectrum reconstruction from Young's double-slits interference pattern using the maximum entropy method," Opt. Lett. **33**, 2341 (2008).

1. Introduction

Coherent diffractive imaging (CDI) is a rapidly evolving field that enables diffraction limited resolution microscopy and quantification of the complex transmission through a specimen. CDI, also known as lensless imaging, is based on the retrieval of a complex sample structure from a measurement of scattered radiation intensity from a coherently

#258186 Received 8 Feb 2016; revised 9 Mar 2016; accepted 10 Mar 2016; published 8 Apr 2016

illuminated sample out of the imaging plane. Lensless imaging is mainly used in short wavelength spectral regions such as extreme ultraviolet (EUV) and X-ray, where high precision imaging optics are difficult to manufacture, expensive and experience high losses. CDI using a single diffraction pattern was firstly introduced in the X-ray synchrotron community [1] as a coherent diffraction based microscopy method for aperiodic samples using additional information about compactness of the sample. In the last decade, a more modern and powerful CDI method for reconstruction of extended samples known as ptychography was introduced [2–5]. The ptychography method is based on illuminating multiple overlapping regions of a sample with a spatially limited beam. Compared to traditional CDI, the redundant information from the overlapping regions makes ptychography significantly more robust.

Theoretically, CDI promises diffraction-limited resolution; however in practical applications the resolution is more often limited by systematic errors than low signal to noise ratio. Systematic errors caused by illumination can be separated into two main groups: errors due to low coherence of the beam, and those due to low temporal stability. Several different relaxation methods have been proposed to deal with the effects of limited coherence [6–11]. However, these methods do not consider errors due to illumination changes over the scan duration.

2. Reconstruction method

In this letter, we present an extension of the ptychography method that enables relaxation of the real space overlap constraint. We call this method orthogonal probe relaxation ptychography (OPRP). OPRP makes possible ptychographic reconstruction using time-varying probe illumination, for example caused by low pointing and intensity stability of the illumination beam or small errors in the sample position. Generally, no additional prior knowledge except the standard overlap constraint is needed to apply the OPRP method, however additional constraints can be beneficial.

The ptychography method [4] searches for a solution in the form of a decomposition of the exit-wave ψ into a complex illumination probe $P(\mathbf{r})$ that is assumed to be identical for whole dataset, and a complex object $O(\mathbf{r})$ that is shifted by a known distance $\mathbf{R}_j$ with respect to the probe for each measured diffraction pattern I_j. In the case of an optically thin specimen, the interaction between the probe and the object can be described as

$$\psi_j(\mathbf{r}) = P(\mathbf{r})O(\mathbf{r}+\mathbf{R}_j) \quad . \tag{1}$$

The exit wave $\psi_j(\mathbf{r})$ propagates to the detector, where the phase information is lost. The measured intensity I_j can be expressed as

$$I_j(\mathbf{q}) = |\Psi(\mathbf{q})|^2 = |\mathfrak{F}(P(\mathbf{r})O(\mathbf{r}+\mathbf{R}_j))|^2 \quad , \tag{2}$$

where Ψ is the Fourier transform of the exit wave ψ_j and q is the transverse component of the scattered wave vector. The exact method of solving this phase retrieval problem depends on the numerical algorithm used. Most of the currently implemented algorithms are projection-based methods [4, 5, 12] that search for a solution that satisfies two constraints. The first is called the modulus constraint, which ensures that exit wave

#258186 Received 8 Feb 2016; revised 9 Mar 2016; accepted 10 Mar 2016; published 8 Apr 2016

propagated on the detector plane complies with modulus of the measured electric field

$$\hat{\Psi}_j(\mathbf{q}) = \frac{\sqrt{I_j(\mathbf{q})}}{|\Psi_j(\mathbf{q})|}\Psi_j(\mathbf{q}) \tag{3}$$

The second constraint enforces equality of the object in the overlapping regions and consistency of the probe.

However, variable illumination caused, for example, by beam movements across the illumination-forming optics effectively results in a slightly different probe for every diffraction pattern and thus the assumption of probe constancy for all scanning position Eq. (1) is not valid. We propose relaxation of the real-space constraint of the ptychography method and thus enable reconstruction with a slightly varying illumination probe.

In ptychography, the probe function must be separable from the object function. This is not possible if an entirely independent reconstruction of the illumination probe is allowed for every scanning position. However, if the beam movements can be considered sufficiently small, then we assume that the illumination function can be approximated as a coherent sum of several orthogonal modes. It has already been shown that one of the advantages of the ptychography method is its ability to recover additional information such as multiple incoherent modes [9, 13] using redundancy that is provided by the overlap constraint. Here, we show that it is also possible to recover coherently added modes. Reconstruction of multiple incoherent modes is based on the fact that each mode is propagated independently and all modes are incoherently summed at the detector plane $I \sim \sum |\Psi_i|^2$ and thus the single mode modulus constraint Eq. (3) is no longer valid and the additional modes are recovered in order to satisfy the incoherent modulus constraint. On the other hand, coherently added modes ($I \sim |\sum \Psi_i|^2$) satisfy the modulus constraint while the the real-space overlap constraint is invalid. This is the reason why a different method must be used to find the optimal decomposition in the real-space that will be able to satisfy the overlap constraint.

The common projection based ptychography algorithms (e.g. extended ptychographic iterative engine (ePIE) [14] and Difference Maps (DM) [5]) are designed to find a single average probe for all positions. Instead of this, the OPRP method modifies the projection algorithms to reconstruct a separated probe for each scanning position. In every iteration, the reconstructed probes are linked together by a projection into a lower n-dimensional space given by a singular value decomposition (SVD) truncated into n orthogonal modes U (eigenprobes). We have used the fast randomized SVD method presented in Ref. [15].

$$[U,S,V] = \mathrm{tsvd}(P,n) \tag{4}$$

The lower dimensional representation $\hat{P}$ of the reconstructed probes is defined by the matrix product of the orthonormal modes U, diagonal matrix of singular values S and complex conjugated orthonormal evolution matrix V

$$\hat{P} = USV^* \quad . \tag{5}$$

The low dimensional projection to $\hat{P}$ provides sufficient information propagation between each probe reconstruction to constraint the reconstruction if the number of modes

#258186 Received 8 Feb 2016; revised 9 Mar 2016; accepted 10 Mar 2016; published 8 Apr 2016

is significantly smaller than the number of the scanning positions. Despite this shared probe constraint, the ePIE based OPRP method remains robust to trapping in local minimas thanks to the serial constraint application on the object function [14]. The ability to recover higher order (low intensity) eigenprobes can be further improved if a relaxed version of the lower dimensional space projector [Eq. (5)] is used

$$P^{(j+1)} = \alpha P^{(j)} + (1-\alpha) USV^* \quad , \tag{6}$$

where $0 \leq \alpha < 1$ is a relaxation constant chosen here as 0.5 and j denotes iteration number. The relaxed constraint is particularly important for the DM algorithm, where it provides better stability and thus avoids divergence when each scanning position uses different probe. The orthogonality and limited number of the modes U are generally sufficient constraints to provide stable and repeatable solution for aperiodic samples, however additional constraints can be beneficial.

The OPRP method allows us to correct only illumination changes between subsequent scanning positions. Variations happening during the exposure time effectively result in decoherence effects [16] and lower the visibility of the diffraction pattern. This can be accounted for using some of the relaxed modulus constraint presented in Refs. [6, 9].

3. Experimental results

The OPRP method was tested in two different experiments. The first proof of concept experiment was performed using illumination by a HeNe laser beam at 633 nm [Fig. 1(a)]. In the next step, the method was tested for a reconstruction of a dataset from a high harmonic generation (HHG) imaging setup at 29 nm wavelength [Fig. 1(b)].

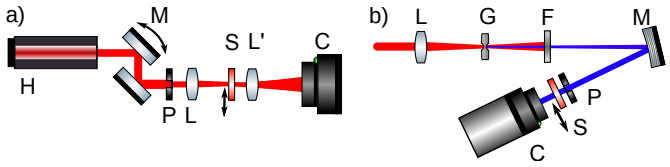

Fig. 1. The schema a) shows our visible light ptychography setup. The HeNe laser beam is deflected by a motorized mirror M, cropped by a pinhole P and projected on a sample S using lens L. The scattered light is collected by a microscope lens L' (NA=0.4) and demagnified on to a camera C that is placed near to the Fourier plane. The schema b) shows the HHG setup. The lens L focuses the IR beam on a gas cell G. The generated EUV light is separated from the fundamental beam by an aluminum filter F. The EUV light is partly spectrally filtered by multilayer mirror M, focused on a pinhole P and propagated on the sample S. The diffracted light is collected by an EUV sensitive camera C. More details can be found in Ref. [17].

Figure 1 shows a ptychography test setup used to benchmark our method. In order to generate a variation of the illumination probe for each scanning position, the pointing direction of the laser beam was slightly modified by the motorized mirror B [Fig. 2(b)]. This resulting beam displacement across the pinhole was comparable with the beam width. In order to reliably compare the gain of the proposed method, two subsequent

#258186 Received 8 Feb 2016; revised 9 Mar 2016; accepted 10 Mar 2016; published 8 Apr 2016

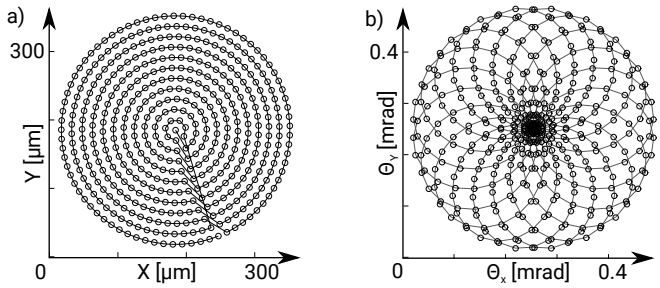

Fig. 2. a) Double spiral probe position scanning path used for the HeNe experiment showing all 463 scanning positions. Figure b) shows desired angular beam deflections used to simulate low pointing stability in the HeNe experiment simulating roughly Lorentz distribution of the beam deflections.

ptychography scans of the same area were collected. Note that the knowledge of the mirror position was not used anywhere in the reconstruction process.

Two types of datasets were collected, one with a actively deflected beam and the second one with stable illumination. Each ptychography scan consisted of 463 positions with 30 μm step size with illumination probe size about 140 μm, in order to get linear overlap of 80%. We have used carbon dust particles deposited on a glass slide as a test object to compare the reconstruction quality.

Figure 3(a) shows the reconstruction of the object using a standard ePIE method when the illumination probe remained stable. Figure 3(b) shows the reconstruction, using the OPRP method, of the object illuminated with a probe that was actively disturbed by moving it during the scan using a motorized mirror. Reconstructions 3(a) and 3(b) are almost identical despite the significant perturbation of the probe in the dataset used in 3(b). Figure 3(c) shows the results of trying to reconstruct the dataset taken using an actively disturbed probe beam using standard ePIE. Despite the high stability and robustness of the standard ePIE method, it was unable to recover the imaged object from the data effectively . The DM method (not shown) was not also able to converge to any consistent image from this dataset. All reconstructions were starting from the same initial guess, and the probe reconstruction started 10 iterations after the object reconstruction. The reconstruction reached convergence after roughly 1000 iterations.

Reliability of the reconstruction was compared using the Fourier ring correlation method (FRC) [18]. Figure 3(d) shows slight reduction in the FRC between Figs 3(a,b) compares to two independent datasets with steady illumination. Slightly lower FRC was expected because the illumination changes were intentionally chosen relatively large in order to show the full potential of our method.

Figure 4 represents the first seven reconstructed eigenprobes with their normalized singular values S and their normalized complex spatial evolution V. The beam position was smoothly changed between exposures to demonstrate the reliability of the reconstructed spatial distribution [Fig. 4)], however it is important to stress that no prior knowledge about the evolution of the beam position is used in the reconstruction in Fig. 4(b).

In order to show that the proposed correction method is also applicable to real

#258186 Received 8 Feb 2016; revised 9 Mar 2016; accepted 10 Mar 2016; published 8 Apr 2016

ptychography experiments with short wavelength illumination, we have applied it to datasets collected from a HHG-based CDI imaging setup [17, 19] [Fig. 1(b)]. Partly monochromatized coherent illumination centered at 29 nm wavelength was produced by a nonlinear interaction between a high peak power driving IR laser and argon gas. The pointing stability of the HHG beam is 0.5-2μm per hour at the pinhole position and it is mostly inherited from the properties of the driving laser beam. The produced EUV light is focused on a 10 μm diameter pinhole by a single multilayer mirror creating a spot size of around 15 μm FWHM on the pinhole. The ptychography scan contained 395 scatter patterns with a 3 μm step size and 10 μm scanning pinhole resulting in a linear overlap of 70%. The scanned sample is approximately 200 nm thick biological material containing mouse hippocampal neuron cells grown on a 50 nm thick silicon nitride foil. The total data acquisition time was 4 hours and during that time the EUV beam was slowly moving over the pinhole, mainly due to pulse length variations of the driving IR laser. The reconstruction is shown in Fig. 6. The overall reconstruction

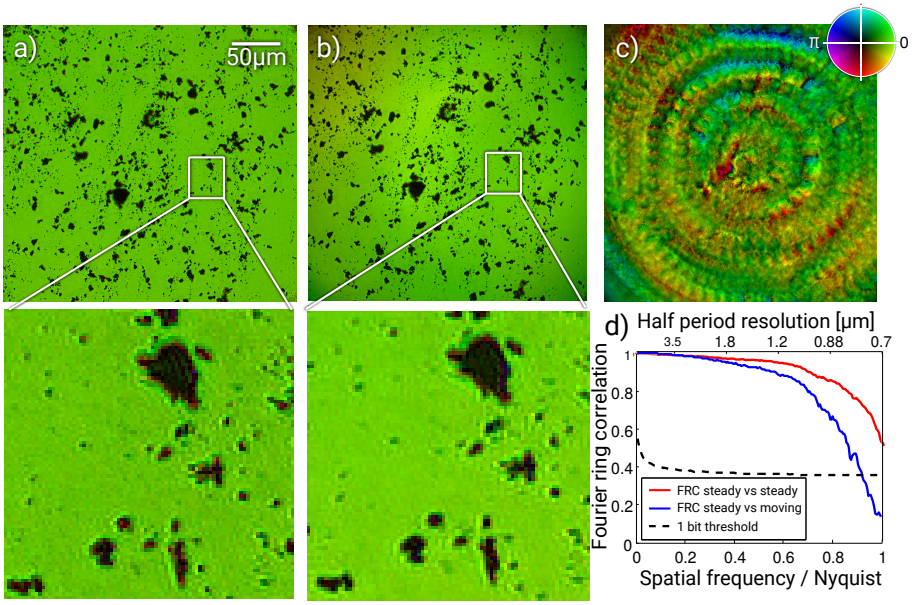

Fig. 3. Reconstructions of graphite particles shown in hue-saturation-value (HSV) complex colorscale. Image a) shows a reconstruction of the dataset with stable illumination using the standard ePIE method. Image (b) shows a reconstruction of the same sample illuminated with an actively disturbed probe, and reconstructed using the OPRP method. Image (c) shows reconstruction after illumination with an actively disturbed probe performed using the standard ePIE algorithm. The reconstruction quality of (b) is comparable to reconstruction (a) even though in image (b) the probe is actively disturbed, while in (a) the probe is stable. Reconstruction (b) shows significant improvement compared to (c), where the standard ePIE method was used on an actively disturbed probe. The last image (d) shows Fourier ring correlation (FRC) between images (a) and (b) compared to two reconstructions of independent datasets with steady illumination (red).

#258186 Received 8 Feb 2016; revised 9 Mar 2016; accepted 10 Mar 2016; published 8 Apr 2016

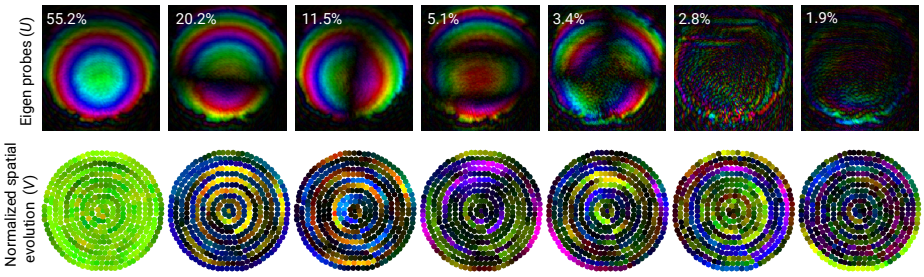

Fig. 4. The first row shows the reconstructed eigenprobes U_i in HSV complex colorscale and their relative singular values intensity $|S_i|/\sum|S_i|$ in percents. The second row shows complex evolution V_i of each eigenmode U_i during the scan [Fig. 2(a)] in complex HSV scale. This representation was used to demonstrate that the modes distribution is dominated by the illumination modulation [Fig. 2(b)]. Diameter of the illumination probe is roughly 140 μm. (See Fig. 8 in the Appendix).

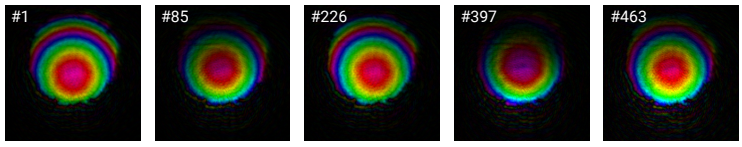

Fig. 5. Examples of the illumination probe reconstructions for several different positions. See Visualization 1 for an animation of the reconstructed probe.

quality from the ePIE [Fig. 6(a)] and OPRP based on ePIE [Fig. 6(b)] is comparable. However, the detailed image shows a number of differences. Thick and thus fully non transparent regions of the cells (1,4,6) contain many artifacts in the standard ePIE method. Small high contrast particles (e.g. next to numbers 2,5) are blurred or missing when standard ePIE was used. Moreover, sharp edges of glioma cells and dendrites connecting the neurons (e.g. connection line above number 3) are sharper and more pronounced when OPRP was used. The reconstruction of the corresponding eigenprobes is shown in the Fig. 7. Because the HHG beam was relatively stable and the ePIE method is very robust, OPRP mainly reduces artefacts near to the resolution limit.

In order to obtain high quality reconstruction, additional modulus constraint relaxation methods were implemented. The PolyCDI method [8, 19] was used to include the broadband HHG illumination in the reconstruction and multimodal ptychography [9] was used to correct the lower diffraction visibility. The pixel scale in both experiments was initially estimated from the experimental geometry, and then further refined by a cross-correlation based method [20] during the reconstruction. Note that no prior knowledge except the HHG spectrum was needed for any of the results presented. The HHG spectrum was measured using a Youngs double slit based spectrometer [19, 21] with the same setup used for ptychography prior to the experiment.

#258186
Received 8 Feb 2016; revised 9 Mar 2016; accepted 10 Mar 2016; published 8 Apr 2016

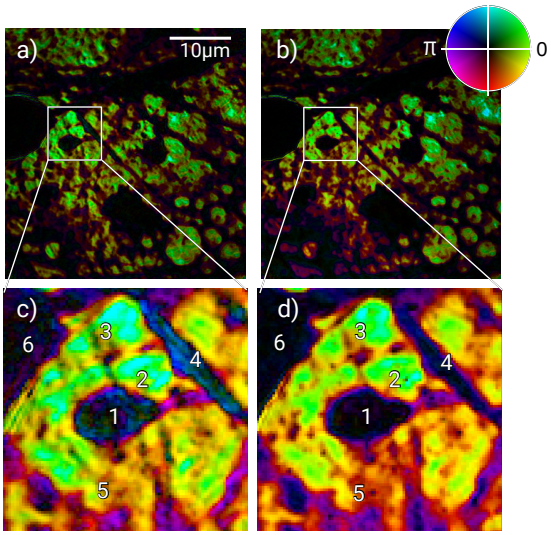

Fig. 6. Ptychography reconstruction of a biological sample. (a) standard ePIE method (b) improved OPRP based on ePIE method. Images (c) and (d) show expanded and contrast enhanced regions of (a) and (b) with details of the neurons and its dendrites. The numbered areas indicate some of the regions where the OPRP method is seen to improve the reconstruction. Details are given in the text.

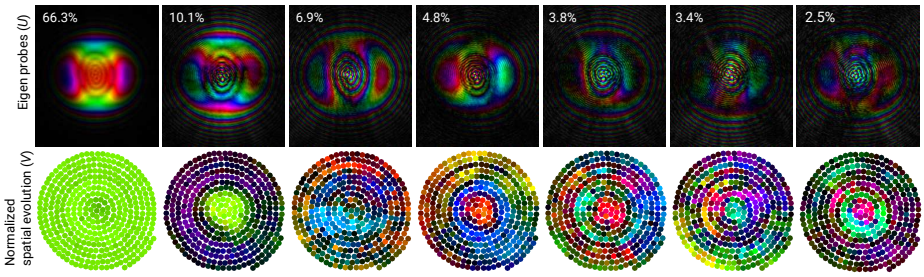

Fig. 7. The first row shows the reconstructed eigenprobes U_i of the HHG illumination and their relative amplitudes $|S_i|/\sum|S_i|$ in percents. The second row shows a complex evolution V_i of each eigenmode U_i during the spiral ptychography scan. The diameter of the illumination probe is roughly 11 μm.

4. Conclusion

The presented technique of orthogonal probe relaxation ptychography shows that relaxation of the real-space overlap constraint is beneficial particularly for experiments with limited stability of the illumination wavefront, however it can be provide superior results in any ptychography reconstructions, where sample or illumination drifts are present. The number of eigen-probes should be sufficiently smaller than the number of scanning positions, however the maximal value depends on the settings of the experiment and complexity of the sample. We have shown a microscopy application in

#258186
Received 8 Feb 2016; revised 9 Mar 2016; accepted 10 Mar 2016; published 8 Apr 2016

the EUV range, however the idea is generally applicable to any wavelength and any configuration of ptychography setup or other scanning CDI methods. Also, we have demonstrated that additional relaxation methods can be used in combination with our method. Variable probe ptychography has potentially even larger application, due to reciprocity of the probe and objects, the variable probe method also naturally correct small errors in the object position and thus automatically include subpixel object shifts of the object, and correct for small position drifts of the piezo motors. The additional time needed to solve the OPRP is between 10-30% of the iteration time in our GPU based ePIE implementation.

Appendix

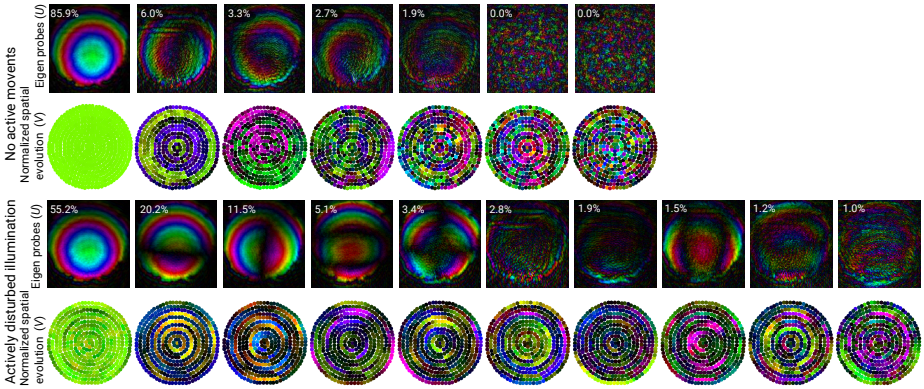

Fig. 8. Reconstruction of all the modes that OPRP method was able to recover for the steady dataset (1th and 2nd row) and the actively disturbed dataset (3rd and 4th rows). The OPRP method was able to recover beam movements and subpixel shifts even for the steady dataset. The beam movements were mostly caused by thermal drifts during the ptychography experiment. If the modes are too weak (e.g. eigenprobes 6 and 7 in the first row), then their relative intensity $S_i/\sum S$ is effectivelly zero.

Acknowledgments

This work builds on the investment and research from the EPSRC Basic Technology grant GR/R87307/01. M.O. acknowledges financial support from the EU FP7 Erasmus Mundus Joint Doctorate Programme EXTATIC under framework partnership agreement FPA-2012-0033 and R.C. acknowledges the EPSRC studentship. The K5200 graphics card used for this research was donated by the NVIDIA Corporation. The data for this work is accessible through the University of Southampton Institutional Research Repository (DOI: 10.5258/SOTON/381931).